2018 IEEE-RAS 18th International Conference on Humanoid Robots (Humanoids)
Beijing, China, November 6-9, 2018

The Magneto-thermal Analysis of A High Torque Density Joint Motor for Humanoid Robots

Wu Zhang[1], Zhangguo Yu[2,3], Xuechao Chen[2,3] and Qiang Huang[2,3]

Abstract— **The high power capacity of humanoid robot is desired for application of running or jumping motions, and the new generation robot formulate the need for a low-mass high-torque motor. A frameless motor has been designed by the group, it is very important to calculate the thermal field of the motor and get the conclusion for the choice of the motor parameters. The magneto-thermal coupling analysis of the motor was carried out based on the thermal network by the iterative calculation. By using the equivalent thermal network method, the elements copper loss and core loss is coupled into elements in thermal analysis by keeping the same mesh structure between magnetic and thermal analysis. Other losses such as air friction loss, rotor loss are included in the model. A temperature rise calculation program was written and different position temperature distribution was obtained. In the meantime, the steady-state temperature of BLDC was calculated by using the finite element method (FEM). The experimental results show that, the actual torque performance of the motor can reach the target of our design, at last, temperature calculation results obtained from two different methods were compared with experimental data, and the correctness of the calculation model is verified.**

I. INTRODUCTION

Improvement of performance of robots has necessitated technological advances in control algorithms, mechanical structures, and electric machines. The humanoid robot joint electromotive motor is used in permanent magnet brushless DC motor which is studied as a key point in recently [1][2]. This kind of permanent magnet motor eliminates the shortage of DC motors, at same time, with the characteristics of low consumption, compact structure, high efficiency and high reliability [3][4]. The Fig. 1 is the BHR-6 robot which is built by the group[5][6], the robot achieve walking, falling, crawling, and rolling. The group has the goal of building the faster humanoid robot, even running and jumping, so it presented challenges in the area of electric machinery in particular. One of the limitations in achieving the goal is the torque used to power the robot, as well as the mass and power dissipation. The Group want to improve torque and reduce the gear requirement, therefore, it is optimal to high torque density and low gear ratio requirement, these limitations formulate the need for a low-mass high-torque motor.

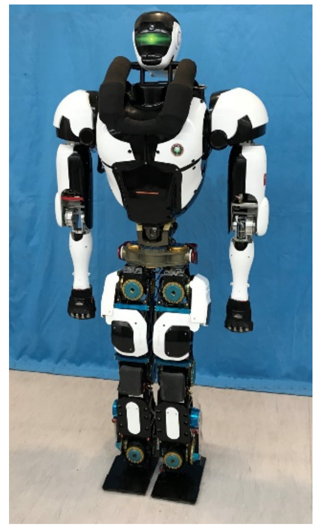

Fig. 1. BHR-6 robot

A frameless permanent magnet brushless DC motor with fractional slot concentrated winding has been designed by the Group. While working at the rated current, the rated torque of the motor output is 1.25 Nm and the weight of the motor is 342g, therefore the torque density of the designed machine is 3.65Nm/kg, moreover, the peak torque of the motor is 4.2Nm. Fig. 2 shows the data which is collected from some commercial motors such as Maxon motors and Kollmorgen motors and Parker motors to evaluate the scaling predictions. From Fig. 2, the torque density of the commercial motors which used by the Group is no more than 2.6Nm/kg. Because the continuous torque represents the motor thermal characteristics, so it is used as a representative metric [7][8]. The torque data of the motor which is designed in this paper is compared with the torque data which has been shown in Fig. 2. From the result, the torque density is two to three times than that of the commercial motor currently used by the Group.

The flux density and the current density of the motor must be designed more higher, at the same time, the temperature in the motor is higher. So it is very important to calculate the thermal field of the motor and get the conclusion for the choice of the motor parameters. Reference [9], thermal network method and finite element method were respectively used to calculate the temperature distribution of automotive induction motors, and the calculation results were verified.

This work was supported in part by the National Natural Science Foundation of China under Grant 61320106012, 61533004 and 91748202.

[1]Beijing Advanced Innovation Center for Intelligent Robots and System, Beijing Institute of Technology.
[2]Intelligent Robotics Institute, School of Mechatronical Engineering, Beijing Institute of Technology.
[3]The Key Laboratory of Biomimetic Robots and Systems, Beijing Institute of Technology.
Corresponding author: Wu Zhang
1zhangwu@163.com

Reference [10], the temperature of the fixed-frequency dual-rotor permanent magnet wind turbine was calculated by means of thermal network. The reference [11] proposed that the heat network and loss of the fluid network were combined to calculate the temperature rise of the synchronous generator with an empty cold water wheel. Reference [12] conducted joint simulation analysis of electromagnetic and thermal models of permanent magnet motors and induction motors. Reference [13] studies the thermal field of a high speed generator using the thermal network method, and obtains the average temperature rise of each component. Reference [14], the fluid-solid coupling method was used to analyze the temperature rise of permanent magnet motor, and computational fluid dynamics method was used to analyze the flow and heat transfer of air gap and end fluid. Reference [15] presents the criteria of the pole-slot numbers combination of the interior and surface permanent magnet synchronous machines with fractional-slot concentrated windings.

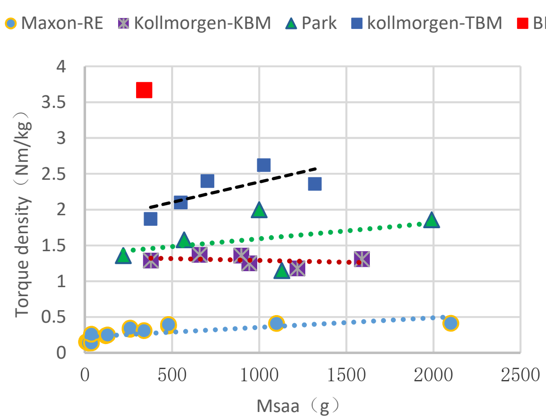

Fig. 2. Torque density contrast

A high torque density joint motor for humanoid robot is studied by the Group in this paper. In section II, the influence of key parameters on electromagnetism performance is analyzed, including the influence of polar arc coefficient and air gap length on torque and thermal load. In section III, the thermal network analysis model of the motor is established. The temperature rise of the motor is simulated by thermal network method and finite element method respectively. In section IV, a prototype is fabricated, and the experimental platform of the prototype system is built. The torque performance and the temperature rise of the motor are tested.

II. ANALYSIS OF KEY PARAMETERS

The performance of the motor is affected by air gap length and the polar- arc coefficient of permanent magnet, here, the finite element analysis method has been used to establish the analysis model of the motor which is shown as Fig. 3. Simulation of motor performance under different parameters is carried out, and the variation trend of the torque and thermal load of the motor with the change of parameters is summarized. From Fig. 4, in the case of air gap is 0.2 and 0.3, the polar arc coefficient increases while the torque decreases, it is because the magnetic field is saturated. And while the air gap is 0.4, 0.5 and 0.6, the torque is increased with the increase of polar arc coefficient, it is because of the large magnetic resistance of air gap, the magnetic density is decreased, therefore, has not caused magnetic density is not saturation in the case of the polar arc coefficient is greater than 0.75. From Fig. 5 the thermal load is decreased as the polar arc coefficient is increased, it's because the magnetic flux goes up and the power stays the same, the increase of the magnetic load reduces the electric load, so the heat load goes down. To sum up, for this type of motor, the polar arc coefficient should be between 0.73 and 0.76.

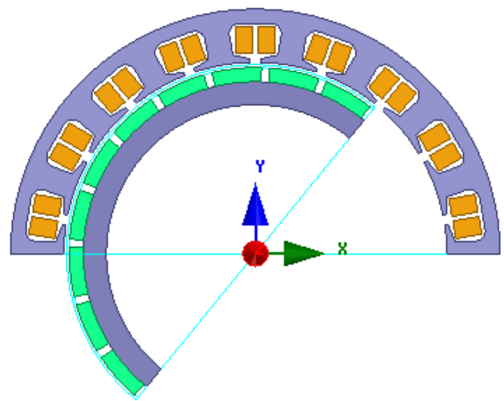

Fig. 3. Surface mounted magnetic pole structure

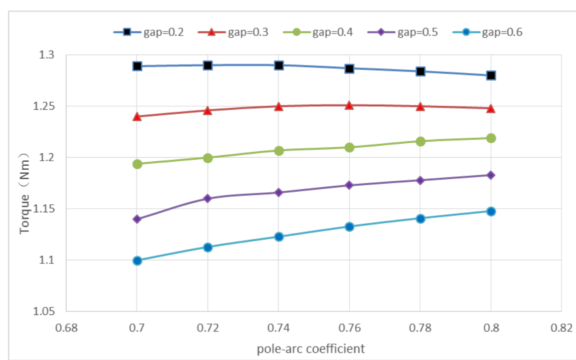

Fig. 4. The varies of torque with polar arc coefficient under different air-gap

III. LUMPED PARAMETER THERMAL NETWORK MODELING AND ANALYSIS OF TEMPERATURE RISE

A. Lumped parameter thermal network modeling

Radial modeling of the motor is shown as the Fig. 6, the heat source of the stator is produced by the stator teeth and yoke, the heat of the conductors in the slot consists of three heat sources. In order to calculate the uneven phenomenon of temperature rise in the slot, the heat of the winding is equivalent to three RC network series, calculate the temperature difference in the slot equivalent to a simplified

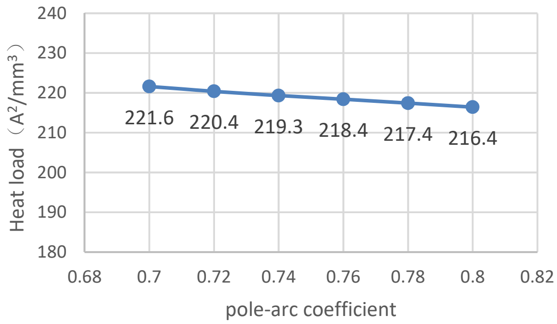

Fig. 5. The varies of thermal load with polar arc coefficient

layered structure. The heat in the stator and the slot is radially transmitted to the outside of the housing by the stator, and then, dissipated by convection of air. The heat source of rotor represents the eddy loss of permanent magnet, the rotating air on the permanent magnet surface is calculated by equivalent thermal resistance or heat transfer coefficient. On the one hand, permanent magnet heating is transmitted from the rotor yoke to the outside through the motor shaft, and on the other hand, when the surface temperature is higher than the stator tooth top, air gap may transfer heat to the stator, and if the surface temperature is lower than the stator tooth, the heat is transferred from the stator to the permanent magnet.

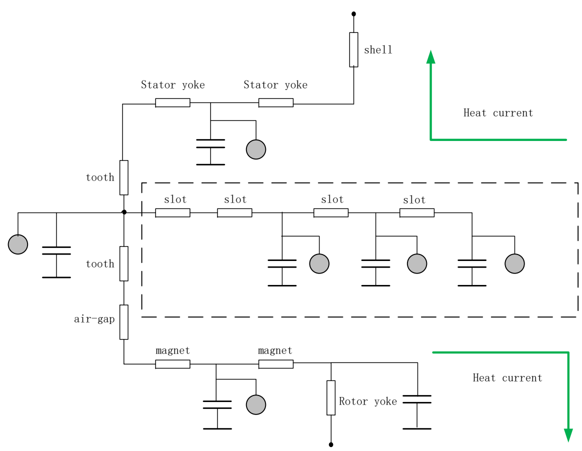

Fig. 6. Radial heat transfer diagram of motor

Thermal path parameters can be calculated from Eq. (1)-(6), here, h is convective heat transfer coefficient, S is surface area, A is Cross-sectional area, λ_v is longitudinal thermal conductivity of materials, d is the air gap length, l_0 is the thickness of the core, D_1 and D_2 is diameter of bearing inner and outer ring, ω is bearing width.

$$R_{Cu-air} = (hS)^{-1}/2 \tag{1}$$

$$R_{air-Cap} = (hA)^{-1}/2 \tag{2}$$

$$R_{Meg-Fe} = d/(\lambda_v S) \tag{3}$$

$$R_{Fe-air} = (hA)^{-1}/2 + l_0(\lambda_v A)^{-1} \tag{4}$$

$$R_{shf} = l_{end}(\lambda_v A)^{-1}/2 + l_0(\lambda_v A)^{-1} \tag{5}$$

$$R_{Bear} = d[(\lambda_v \pi D_1 \omega)^{-1} + (\lambda_v \pi D_2 \omega)^{-1}] \tag{6}$$

B. Temperature calculation of the motor

The heat network model is established as shown in the Fig. 7, the magneto-thermal coupling analysis of the motor was carried out based on the heat path model by the iterative calculation. The electromagnetic calculation module is used to calculate the loss of each part of the motor at normal temperature, then, the loss value is imported into the temperature calculation module to calculate the temperature distribution of each area of the motor, more over we come back to the electromagnetic module to calculate the loss value of each part of the motor under the temperature distribution .The above process is iterated to obtain the convergence of motor temperature distribution and the loss of each part.

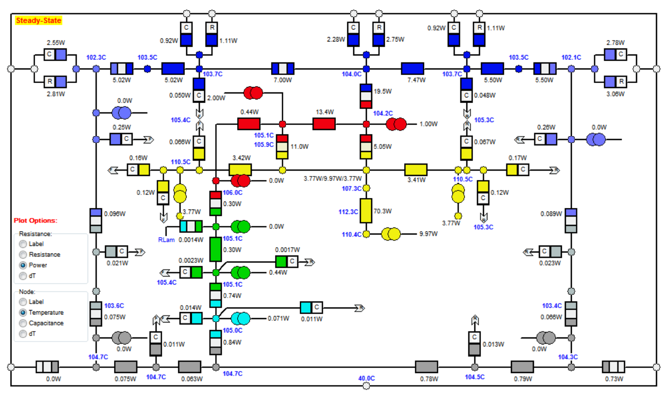

Fig. 7. Lumped parameter thermal network model of the motor

Fig. 8 shows the temperature distribution of each part of the motor after reaching thermal balance calculated by the heat path method, from the Fig. 8, the surface temperature of permanent magnet is 105°C, which will not cause permanent magnet demagnetization. Winding is the main factor of heating during motor operation, it can be seen from the figure that the maximum temperature of the winding is 119.5°C and the average temperature is 117.9°C. Fig. 9 shows the temperature rise of the motor winding after reaching thermal balance by using finite element method, the maximum temperature of the winding is 117°C, and the results of the two methods are consistent.

IV. THE EXPERIMENT

A torque motor is designed, and the prototype is shown in Fig. 10. In order to test the load performance of the prototype and the temperature rise during the operation of the prototype, a motor test platform is built in this paperas shown is Fig. 11. The test platform is mainly consisted of the following parts: the motor to be tested, the driver,

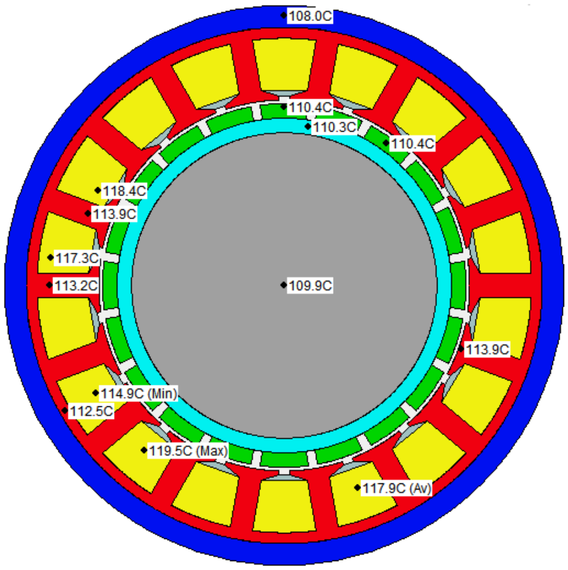

Fig. 8. Temperature distribution of the motor

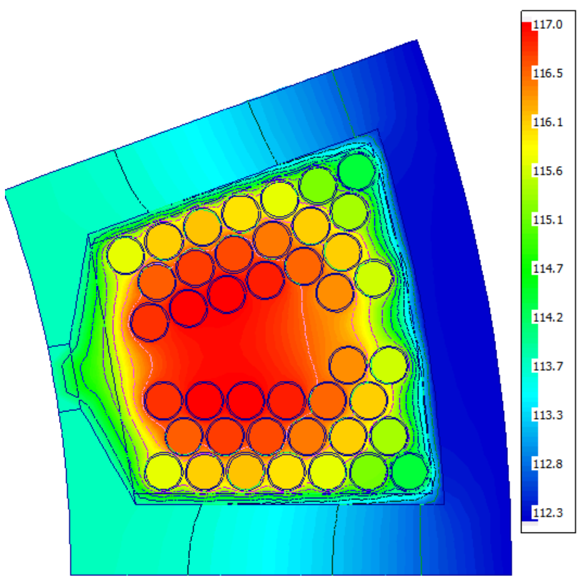

Fig. 9. Temperature distribution of winding

the ac intelligent load, the load controller, the speed-torque sensor, the power analyzer and the temperature measuring instrument.

Fig. 12 is the core loss curve of the motor. From the loss curve, after the motor has been steady running, the core loss is 12.3855w, the vortex loss 9.0513w, the hysteresis loss 3.3342w, total loss is 24.77w at 20°C. The rated power is 275w, therefore the max efficiency of the motor is 90.9%.

Fig. 13 is the induction voltage of the windings. Calculate the current according to the losses which have been shown in Fig. 7:

$$I = \sqrt{\frac{P_{cu}}{3R_{\varphi}}} = \sqrt{\frac{24.77}{3 \times \frac{0.655}{2}}} \approx 4.95\text{A}$$

Fig. 10. Prototype machine for test

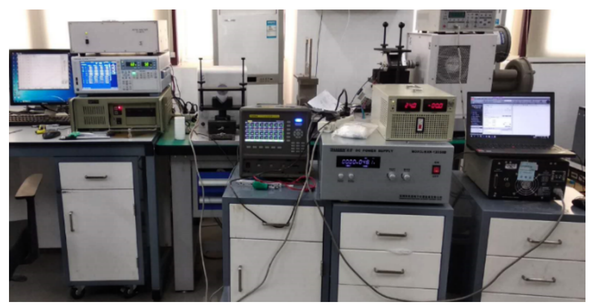

Fig. 11. The experiment platform

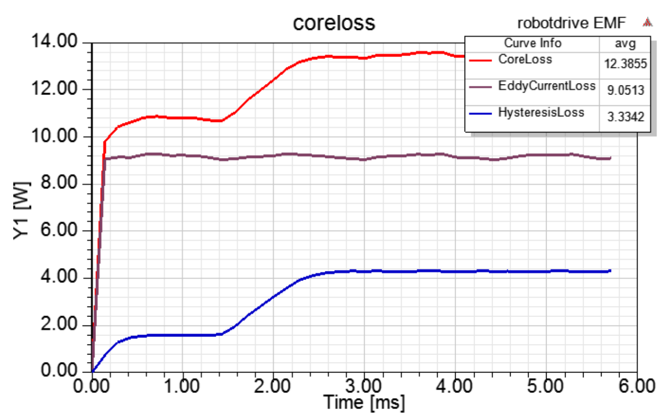

Fig. 12. Core loss curve

$$p\psi_f = \frac{T}{I} = \frac{T}{\sqrt{3}I_q} = \frac{1.25}{1.732 \times 4.95} = 0.146$$

Therefore, the no-load line induction voltage is

$$E = \omega\psi_f = \frac{2\pi pn}{60} \times \frac{p\psi_f}{p} \approx 32\text{V}$$

The results computed by the analytical method are consistent with the results computed by the experimental data as shown in Fig. 13, which prove the feasibility of the design method.

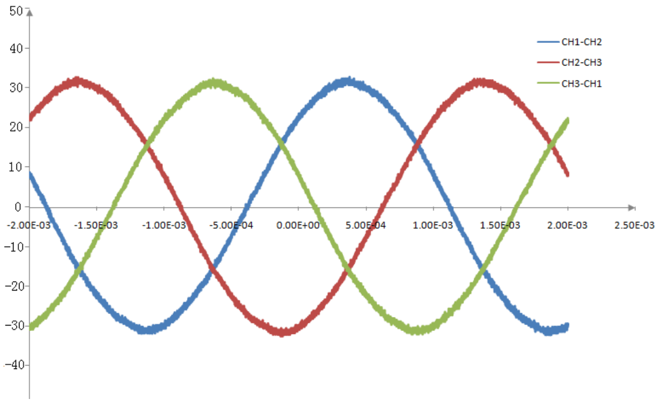

Fig. 13. Induction voltage of the windings

The motor worked at the rated voltage by the driver, the peak torque of the motor is 4.2Nm, based on the experimental platform as shown in the Fig. 11, from 0Nm to 4.5Nm, increase the load every 5 seconds, and each additional step is 0.2Nm. Fig. 14 is the torque-current curve of the motor, experimental results show that, the actual torque performance of the motor can reach the target of our design.

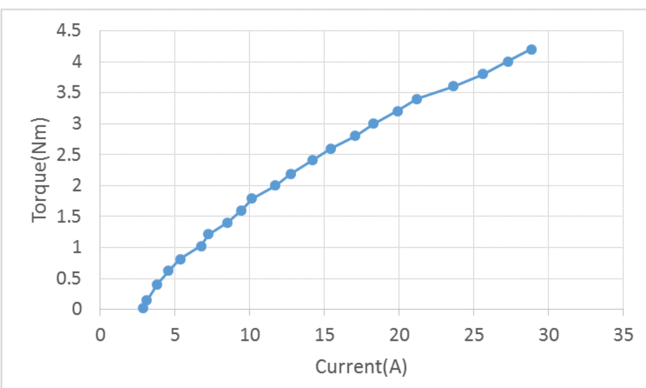

Fig. 14. Torque-current curve

The heat-sensitive resistance PT100 is embedded at the end of the winding, and the motor is cooled by natural cooling, the actual temperature value of motor winding is displayed by temperature measuring instrument during the operation of the motor. Table 1 shows the temperature which is and obtained by thermal network method and finite element method and experimental values, and the Fig. 15 is the temperature rise curve of the winding. The results of the thermal network method and finite element method are compared with the experimental data, the error of winding temperature is respectively 3.5% and 1.7%, the validity of theoretical calculation is proved, and at the same time, the actual temperature rise of the motor is 115.5°C, the temperature rise of the motor is well, so it can guarantee safe operation under the allowed insulation condition.

TABLE I
CALCULATED RESULTS AND MEASURED DATA

Comparison items	Different ways		
	thermal network	finite element	experimental value
Winding temperature rise °C	119.5	117	115.5

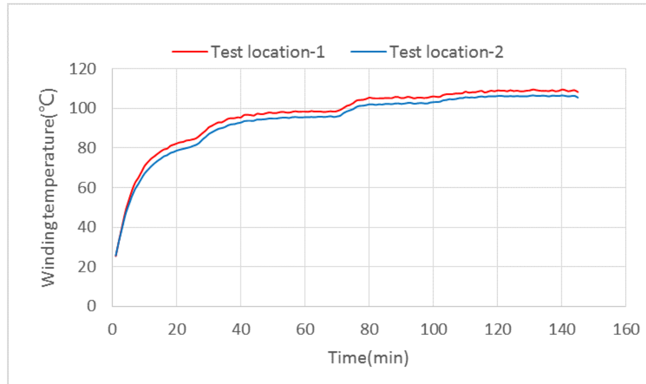

Fig. 15. Temperature rise curve

V. CONCLUSIONS

A high torque density joint motor for humanoid robot is designed by the group, the influence of key parameters on electromagnetism performance is analyzed, and it has important significance to electromagnetic design for BLDC with similar rotor structure. The thermal network model is established, the magneto-thermal coupling analysis of the motor was carried out, the maximum temperature of the winding is 119.5°C and the average temperature is 117.9°C. By using finite element method, the maximum temperature of the winding is 117°C, and the results of the two methods are consistent. Experimental results show that, the actual torque performance of the motor can reach the target of our design, the torque density of the designed motor is 3.65Nm/kg. The actual temperature rise of the motor is 115.5°C, it can guarantee safety operation under the allowed insulation condition. In the future, we will apply this motor to our own humanoid robot, so as to improve the dynamic performance of the robot.

ACKNOWLEDGMENT

The authors would like to thank Dr. Fei Meng and Dr. Huaxin Liu, which gave us the valuable suggestions.

REFERENCES

[1] S. Seok, A. Wang, Y. Meng, et al., “Design principles for energy-efficient legged locomotion and implementation on the mit cheetah robot,” *IEEE/ASME Transactions on Mechatronics*, vol. 20, no. 3, pp. 1117-1128, June 2015.

[2] Y. Zhou, H. Li, G. Meng, et al., “Analytical calculation of magnetic field and cogging torque in surface-mounted permanent-magnet machines accounting for any eccentric rotor shape,” *IEEE Transactions on Industrial Electronics*, vol. 62, no. 6, pp. 3438-3447, 2015.

[3] S. Seok, A. Wang, Y. Meng, D. Otten, J. Lang, and S. Kim, “Design principles for highly efficient quadrupeds and implementation on the MIT cheetah robot,” in *Proc. IEEE Int. Conf. Robot. Autom.*, 2013, pp. 33073312.

[4] P. Chen, R. Tang, W. Tong, et al., “Permanent magnet eddy current loss and its influence of high power density permanent magnet synchronous motor,” *Transactions of China Electro technical Society*, vol. 30, no.6, pp. 1-9, 2015.

[5] Z. Zhang, H. Liu, Z. Yu, X. Chen, et al., “Biomimetic upper limb mechanism of humanoid robot for shock resistance based on viscoelasticity,” in *IEEE-RAS 17th International Conference on Humanoid Robotics*, 2017, pp. 637-642.

[6] Z. Luo, X. Chen, Z. Yu, Q. Huang, et al., “Trajectory optimization of humanoid robots swinging leg,” in *IEEE-RAS 17th International Conference on Humanoid Robotics*, 2017, pp. 359-364.

[7] J. Dong, Y. Huang, L. Jin, et al., “Thermal optimization of a high-speed permanent magnet motor,” *IEEE Transactions on Magnetics*, vol. 50, no. 2, pp. 749-752, 2014.

[8] L. Li, J. Zhang, C. Zhang, et al., “Research on electromagnetic and thermal issue of high-efficiency and high-power-density outer-rotor motor,” *IEEE Transactions on Applied Superconductivity*, vol. 26, no. 4, pp. 15, 2016.

[9] W. Jiang, T. M. Jahns, “Coupled electromagnetic - thermal analysis of electric machines including transient operation based on finite-element techniques,” *IEEE Transactions on Industry Applications*, vol. 51, no. 2, pp. 18801889, 2015.

[10] I. Bouzidi, A. Masmoudi, N. Bianchi, “Electromagnetic/thermal design procedure of an aerospace electric propeller,” *IEEE Transactions on Industry Applications*, vol. 51, no. 6, pp. 43644371, 2015.

[11] A. Boglietti, E. Carpaneto, M. Cossale, et al., “Stator-winding thermal models for short-time thermal transients: definition and validation,” *IEEE Transactions on Industrial Electronics*, vol. 63, no. 5, pp. 27132721, 2016.

[12] G. Correa, M. Santarelli, F. Borello, et al., “Flight test validation of the dynamic model of a fuel cell system for ultra-light aircraft,” *Proceedings of the Institution of Mechanical Engineers, Part G: Journal of Aerospace Engineering*, vol. 229, no.5, pp. 917932, 2016.

[13] S. Song, M. Zhang, Y. Wu, “Cooling system design for switched reluctance motor based on analytic calculation of thermal field,” *Electric Machines & Control Application*, vol. 40, no. 9, pp. 6, 2013.

[14] J. Zhang, Y. Jiang, “Thermal analysis of constant frequency double rotor permanent magnet generator based on equivalent thermal network method,” *Transactions of China Electro technical Society*, vol. 30, no. 2, pp. 87-97, 2015(in Chinese).

[15] M. Si, Y. Yang, “The influence of pole-slot match on magneto-motive force with concentrated fractional-slot winding,” *Applied Mechanics & Materials*, vol. 39, no. 7, pp. 12091213, 2013.